NBSIR 74-579 (P)

Metallographic Examination of Cylinder Barrels Made From Aluminum Alloy (A-356) Sand Castings

B. W. Christ

Mechanical Properties Section
Metallurgy Division
Institute for Materials Research
National Bureau of Standards
Washington, D. C. 20234

September 1974

Failure Analysis Report

Prepared for
Naval Ordnance Laboratory
Department of the Navy
White Oak
Silver Spring, Md. 20910

NBSIR 74-579

METALLOGRAPHIC EXAMINATION OF CYLINDER BARRELS MADE FROM ALUMINUM (A-356) SAND CASTINGS

B. W. Christ

Mechanical Properties Section
Metallurgy Division
Institute for Materials Research
National Bureau of Standards
Washington, D. C. 20234

September 1974

Failure Analysis Report

Prepared for
Naval Ordnance Laboratory
Department of the Navy
White Oak
Silver Spring, Md. 20910

U. S. DEPARTMENT OF COMMERCE, Frederick B. Dent, Secretary

NATIONAL BUREAU OF STANDARDS, Richard W. Roberts, Director

REFERENCE: Mr. Ray Wiley
Code 211 Magnetism & Metallurgy Division
Bldg. 24-20
Naval Ordnance Laboratory
White Oak, Silver Spring, Md. 20910
NOL Project Order No. N60921-75-PO 00074
JOB ORDER 551-03091-3SD

I. INTRODUCTION:

A. Nature of the Investigation

At the request of the above reference, the Mechanical Properties Section of the NBS Metallurgy Division undertook a metallographic investigation of some specimens from aluminum alloy sand castings used for cylinder barrels. It was reported to the Mechanical Properties Section that the alloy was A-356. It was also reported that some of these castings exhibited a tendency to crack during machining or test firing, and that tensile specimens taken from some of them exhibited smaller elongations and ultimate tensile strengths than those set forth in the specification. (See Table I.) The objective of this investigation was to identify the causes of the cracking and the anomalously-low mechanical properties. Initial analysis of these materials at NOL suggested that cracking and anomalously-low mechanical properties were somehow related to eutectic melting.

B. Chemical Composition, Heat Treatment and Microstructure

Aluminum alloy A-356 has the nominal composition, Al- 7% Si- 0.3% Mg.[1] "A" designates a premium grade alloy with a maximum of 0.2 wt. pct. iron.[1] This casting alloy is a precipitation hardening material which is solution treated at 980 to 1010°F, cooled with water at 150 to 212°F, then precipitation hardened (or "aged") to a T6 condition by holding at 300 to 320°F for 1 to 6 hours.[2a] The precipitating phase which causes hardening is Mg_2Si.[1b] Iron concentration is kept low to minimize the formation of the embrittling ternary phase, $Fe_2Si_2Al_9$.[1c]

A prominent microstructural feature of the as-cast alloy is the network of silicon particles which solidify at the binary eutectic temperature of 1071°F.[1d] The binary eutectic is composed of primary aluminum solid solution, showing up as the white matrix phase in Figure 1a, and silicon solid solution (which is almost pure silicon), showing up as the network of gray particles in Figure 1a. A close-up of these eutectic silicon particles appears in Figure 1b. The "finger-print" smudge features appearing within the eutectic silicon network of Figure 1 are due to a dispersion of the hardening phase, which is thought to be Mg_2Si.[1b, 1d]

A close-up of one of these features, e.g., Figure 4, has a "pepper-like" appearance. The eutectic silicon network solidifies when the casting solidifies, whereas the Mg_2Si particles form in the solid state during aging. For convenient reference below, a summary of the eutectics which may form in A-356 alloy appears in Table II.

II. MATERIALS AND PROCEDURES:

Material supplied to NBS by NOL came from sand castings which reportedly originated at either of two foundries, Ohio Aluminum Industries or the Wellman Company. Some material, chiefly from Ohio Aluminum Industries, exhibited cracks and anomalously-low tensile properties. Seven as-mounted metallographic specimens of the Ohio material were supplied. (See Table III.) Also, two fractured tensile bars were supplied, one from Ohio material and one from Wellman material. Further, a small segment of an Ohio casting containing a natural crack* near a drilled pin hole was supplied. Finally, a number of photomicrographs resulting from initial metallographic work at NOL were supplied.

Three of the as-mounted metallographic specimens were re-polished and re-etched, and various photomicrographs were prepared. Fracture surfaces of the broken tensile bars were photographed, and one specimen for mounting and polishing was cut from a half of each foundry's tensile bar. The natural crack in the small segment of Ohio material was photographed, then a small piece was carefully cut from it for mounting and polishing so that details of the natural crack could be observed at magnifications of 50 to 250X. The ligament holding the cracked halves of the small segment together was severed during this cutting operation, and the fracture surfaces of the natural crack thus revealed were photographed in the SEM. Finally, Knoop hardness measurements were made on the metallographic specimen prepared from each foundry's tensile bar.

III. RESULTS AND DISCUSSION:

A. Metallographic Specimens Cut From Tensile Bars

The microstructure characteristic of Ohio material appears in Figure 2a, and that characteristic of Wellman material appears in Figure 2b. There is a noticeable difference in the porosity, which shows up as the black regions in each photomicrograph. The pore size appears larger, and the number of pores appears greater in the Ohio material. The cause of this difference in the porosity of the two castings is not clear. The rounded dendrite arms of primary aluminum solid solution projecting into the larger pores of the Ohio material, and the location of these pores, suggest that they are interdendritic shrinkage cavities. The location and shape of the smaller pores in the Ohio material suggest that they may be gas pores.

---

* "natural crack" is defined in Section III-B.

Comparison of Figures 2a and 2b indicates that the microstructure is coarser in the Ohio material than in the Wellman material, i.e., on the average, the white patches of primary aluminum solid solution and the eutectic silicon particles are coarser in the Ohio material than in the Wellman material. This difference is possibly due to the difference in solidification rates, for it is well known that a cast microstructure becomes finer as the solidification rate increases.[3] However, influences on the scale of the microstructure related to the maximum temperature reached during solution heat treatment (see Section III-D) and to sodium additions (see Section III-E) should not be overlooked.

Figures 3a and 3b compare eutectic silicon particles in Ohio and Wellman material, respectively. Not only are the eutectic silicon particles in the Ohio material larger than those in the Wellman material, they are also plate-like, whereas those in the Wellman material are rod-like. (This point is discussed further in Section III-E.) Furthermore, comparison of Figures 3a and 3b indicates that the eutectic silicon network is more continuous in the Ohio material than in the Wellman material. This point can be verified by placing an imaginary line through several silicon particles in the interdendritic regions, then determining the number of intercepts with aluminum solid solution for a fixed line length. On the average, there will be fewer intercepts in the Ohio material than in the Wellman material. This latter feature of microstructure, i.e., the continuity of the eutectic silicon particles in the interdendritic region, is important in the analysis of cracks and the loss of ductility. Essentially, the brittle silicon particles represent an easy-to-fracture phase in the microstructure, and the greater the continuity of the eutectic silicon network, the easier a crack can propagate throughout the microstructure. This point will be discussed further in Section III-B.

The "pepper-like" regions of Mg_2Si appear in the Ohio material as shown in Figure 4a and in the Wellman material as in Figure 4b. Mg_2Si is also evident in Figures 2a and 2b as the dendrite shapes which appear in the regions of primary aluminum solid solution. The size and distribution of Mg_2Si particles seems to be quite similar in both the Ohio and Wellman materials. This observation is consistent with the results of tensile and hardness tests, which showed no significant differences in the yield stresses and hardnesses of the Ohio and Wellman materials. Yield stresses appear in Table I. Furthermore, average hardnesses, as determined by placing a Knoop indenter in the primary aluminum solid solution, were 110 and 106, respectively, for Ohio and Wellman material. These hardness values convert to Rockwell-B values of 53 and 49. A typical hardness impression appears at the top-left in Figure 2a.

B. Relationship of Natural Crack Path to Microstructure

Natural cracks are defined as cracks which were found in the castings. Natural cracks found in various specimens taken from Ohio material almost always followed a path through the silicon-rich interdendritic regions, as shown in Figures 5a and 5b. The crack in Figure 5a is near a specimen surface and runs between two dark regions which may be sand particles trapped in the casting. This is the only near surface crack of this type which was found. The crack in Figure 5a appears at higher magnification in Figure 6. The tendency for a crack to follow a path through the silicon-rich interdendritic regions is evident in the similarity between the wandering nature of the crack path on an as-machined surface, Figure 7, and that of the crack path in Figure 5b.

Figure 8 shows examples of eutectic silicon particles adhering to both surfaces of a natural crack. This feature was observed along the entire crack length. The presence of silicon particles along the crack edge suggests that the crack propagated by fracturing any silicon particles which it could reach. Indeed, the secondary branches of the main crack appearing in Figure 8a show the fracture of silicon particles. This fracture process is vividly illustrated at higher magnification in Figure 8b. The force which propagated the crack probably came from residual stresses in the casting, as well as from applied stresses accompanying machining operations and/or test firings.

It is evident from Figures 5 and 8 that the ease with which a crack can advance throughout the microstructure increases as the continuity of the network of eutectic silicon particles increases, since the silicon particles are a brittle (and relatively weak) phase. The difference in this feature of microstructure between the Ohio and Wellman material, as discussed in Section III-A, is probably the cause of the higher frequency of cracking and the anomalously-low mechanical properties of the Ohio material as reported by NOL. Probably the large interdendritic shrinkage pores in the Ohio material, which were pointed out in Section III-A, facilitate the nucleation of cracks in the interdendritic regions. As mentioned in Section I-A, initial analysis of these materials at NOL suggested that cracking and anomalously low mechanical properties were somehow related to eutectic melting. However, it is not obvious that the features of microstructure in the Ohio material suspected of causing cracking and anomalously-low mechanical properties, namely, a nearly-continuous network of large eutectic silicon platelets in the interdendritic regions and large interdendritic pores, are a consequence of the overheating which causes eutectic melting. (See Section III-D for a discussion of eutectic melting.)

C. Observations of Fracture Surfaces

1. Natural Crack Viewed in SEM

The fracture surfaces of the natural crack were viewed in the SEM. The fracture surfaces exhibited numerous cleavage facets, as is clear from Figures 9a, 9b, and 9c. Observations with the stereographic viewer confirmed that most topographic features on these fracture surfaces were cleavage facets. Very little evidence of dimpled rupture was found.

Since Figure 8 shows silicon particles on both surfaces of the natural crack, it may be inferred from Figures 8 and 9 that the crack propagation mode was principally via cleavage of the brittle and relatively weak silicon particles. The angular voids which appear in Figures 9 probably resulted when silicon particles were pulled out at some stage of the fracture process. The rounded voids appearing in the top left quadrant of Figure 9b probably resulted from the interdendritic shrinkage which occurred during the initial solidification of the casting. The shadowy features appearing in these voids are thought to be dendrite arms of the primary aluminum solid solution.

2. Fracture Surfaces of Tensile Bars

Figure 10 shows the fracture surfaces of a tensile bar machined from each foundry's castings. SEM results appear in Figures 10a and 10b, and optical microscopy results appear in Figures 10c and 10d. The polygonal regions in Figures 10a and 10b are interpreted as evidence of cleavage facets. The larger scale of the microstructural features in the Ohio material as compared to the Wellman material, a feature already noted in Section III-A, is also evident from comparison of Figures 10a and 10b. The region of rounded features appearing in the bottom center of Figure 10a is interpreted as an interdendritic shrinkage pore, with the rounded features presumed to be the arms of primary aluminum dendrites. The chief difference between the optical micrographs, Figures 10c and 10d, is that a larger number and larger size of bright facets appear on the tensile bar made from the Ohio casting. These facets are probably the same cleaved particles of silicon which were pointed out in the discussion of Figures 5, 8 and 9, in Sections III-B and III-C-1.

The presence of bright facets on the fracture surface of the tensile bar made from a Wellman casting, Figure 10d, suggests that cracks also propagate through silicon particles in this material if the stress is high enough (ultimate tensile stress is about 43,000 psi, as compared to about 35,500 psi for tensile bars from the Ohio casting, Table I). However, to reiterate, the main difference between the fracture surfaces in Figures 10a and 10b is the number and size of bright facets, not just their presence. This difference is easily seen on the fracture surface of tensile bars with the unaided eye, as well as with a low-magnification, hand-held magnifier.

D. Eutectic Melting

Eutectic melting is a phenomenon which sometimes occurs in the heat treatment of precipitation hardening aluminum alloys. Available literature[4,5] describes eutectic melting principally for wrought aluminum alloys, but the phenomenon can also occur during the heat treatment of aluminum alloy castings. The microstructural features usually cited as evidence of eutectic melting are rosettes and dark etching grain boundaries.[5] Two consequences of eutectic melting are reduced tensile strength and reduced elongation, i.e., embrittlement. Changes in microstructural features and mechanical properties resulting from eutectic melting are thought to be irreversible.[5]

The type of rosette appearing in the middle of the primary aluminum solid solution in Figure 11a is usually regarded as resulting from solidification of the ternary eutectic, composed of aluminum solid solution, silicon solid solution and Mg_2Si. The expected three phases appear as white, light gray and dark gray regions of the rosette. Features thought to be the same ternary eutectic also appear in Figures 4a, 11b, and 11c although the rosette shape is not pronounced in Figure 11c.

The blade-like particles appearing in Figures 11 are thought to be $Fe_2Si_2Al_9$, a ternary phase of the Fe-Si-Al system.[1c] Blades of $Fe_2Si_2Al_9$ were often observed to connect eutectic silicon particles in the Ohio material, e.g., see Figure 11a, upper left and upper right. Generally, there seemed to be more $Fe_2Si_2Al_9$ blades in the Ohio material than in the Wellman material. The reported iron analyses of castings from both foundries, < 0.05 wt. pct., is well below the 0.2% max. appearing in the specifications for A-356. Thus, embrittlement from iron bearing intermetallic compounds is not likely.

Figures 11 were obtained from Ohio material, namely, the metallographic specimen prepared from a segment of the fractured tensile bar. Rosettes were found in specimens from both foundries, but there was a larger number of rosettes in the Ohio material. It is not clear when the rosettes formed, i.e., during solidification of the casting or during the solution heat treatment.

Figure 12 shows a microstructural feature of Ohio material, the triangular region projecting from a silicon particle, which is interpreted as evidence of melting of the binary eutectic. This eutectic is composed of the terminal aluminum solid solution and the terminal silicon solid solution, and the eutectic temperature is 1071°F.[1b] Binary eutectic melting usually initiates at grain boundaries, and indeed, this is the case in Figure 12. The

expected two phases, etching lightly and darkly, show up clearly in the triangular region. The triangular shape, determined by surface tension, suggests that the binary eutectic melted while the surrounding material was solid. Furthermore, the smaller size of the phases in the triangular region, as compared to the size of the surrounding aluminum solid solution and silicon particles, also suggests that the binary eutectic melted while the surrounding material was solid. For example, the surrounding material could have acted as a heat sink to rapidly cool the triangular region and thereby produce the smaller particle size. It is possible that the melting occurred during a temperature excursion during the solution heat treatment of the Ohio material.

Triangular regions such as that appearing in Figure 12 were not detected in the Wellman material. The small size of the triangular region, and the fine particle size of the phases in it, makes detection of such regions extremely difficult. High magnification, e.g., 1000X, and extremely careful etching are required to reveal such regions.

E. Morphology of Eutectic Silicon Particles in Al-Si Casting Alloys

Eutectic silicon particles can be present in aluminum-silicon casting alloys as platelets or rods.[6] Solidification rates, as well as sodium modification (i.e., addition of about .020% sodium to the casting alloy) are known to influence the morphology of eutectic silicon particles.[7-11] Thus, the difference between the eutectic silicon particles in the Ohio and Wellman materials namely, large, impinging platelets in the former and small, separated rods in the latter (see Section III-A) may be related to solidification rate and sodium modification. The apparently greater continuity of the network of eutectic silicon particles in the Ohio material, as compared to Wellman material, was identified in Section III-B as the difference in microstructures most likely to explain the increased susceptibility of Ohio material to cracking.

An early report[10] about sodium modification indicated that there were problems "in obtaining gas free metal after introducing sodium". Thus, it is possible that the difference in porosity noted between the Ohio and Wellman material (see Section III-A) may somehow be related to the introduction of sodium. The possibility that pores might act as crack nucleation sites was discussed in Section III-B.

IV. SUGGESTIONS FOR NON-DESTRUCTIVE EVALUATION:

During the course of this metallographic investigation, a question arose as to which non-destructive evaluation methods might be used on hardware in the field to evaluate its susceptibility to cracking. Results of this investigation suggest the following possibilities:

1. Polish a metallographic surface of hardware in the field[12] and etch to reveal the nature of the eutectic silicon particles in the interdendritic regions. If the particles were large and platelike, and if the particles formed a nearly-continuous network, it might be suspected that the hardware would be susceptible to cracking. This suggested NDE method would require some development, so that effects on microstructure due to different solidification rates near and remote from surfaces could be recognized.

2. Remove a small sacrifical specimen from a piece of hardware, fracture it and visually examine the fracture surface for bright facets. A large number of large-size facets would be cause for suspecting that the hardware would be susceptible to cracking. (See Section III-C-2.) Again, some development would be required so that effects on fracture surface facets due to different solidification rates near and remote from surfaces could be recognized.

3. Remove a small sacrificial specimen from a piece of hardware and carry out chemical analysis for sodium. A low sodium concentration might lead to the suspicion that the sodium addition intended to promote modification of the eutectic silicon morphology (see Section III-E) was overlooked or improperly handled. Admittedly, some development would be required so that effects on sodium distributions due to differences in solidification rates near and remote from surfaces could be recognized.

Whereas each of these suggested NDE methods provides some information about the susceptibility of a piece of hardware to cracking, it might be best if results from all three suggested methods (and perhaps results from other methods as well) were used as the basis for final decisions about the susceptibility of a piece of hardware to cracking.

V. SUMMARY AND CONCLUSIONS:

A metallographic investigation of some precipitation hardened aluminum castings (A-356) used for cylinder barrels was carried out. The material investigated came from sand castings supplied by two foundries, Ohio Aluminum Industries and Wellman Company. Some material, chiefly from Ohio Aluminum Industries, exhibited cracks and anomalously-low tensile properties. The objective of this investigation was to identify the causes of this behavior. Observations were made with the light microscope and the scanning electron microscope.

The natural crack path in Ohio material was closely related to the microstructure, i.e., natural cracks followed the network of eutectic silicon particles in the interdendritic regions. Eutectic silicon particles were found on both sides of a natural crack, and the fragmenting of silicon particles in the early stages of crack propagation was evident. Numerous shrinkage pores appeared in the interdendritic regions, and it was suggested that these pores served as crack nucleation sites.

The microstructure of Ohio material was noticeably coarser than the microstructure of Wellman material, i.e., the size of primary aluminum dendrites was larger and the size of eutectic silicon particles was larger. Moreover, eutectic silicon particles in the Ohio material were platelike, whereas those in the Wellman material were rod-like. The network of eutectic silicon particles was more continuous in the Ohio material than in the Wellman material. Furthermore, the number and size of pores attributed to interdendritic shrinkage was larger in the Ohio material than in the Wellman material. More evidence of eutectic melting was found in the Ohio material than in the Wellman material, but it was not obvious that the increased susceptibility of Ohio material to cracking and its loss of mechanical properties was a consequence of the overheating which causes eutectic melting. There were no notable differences in the hardening precipitate, Mg_2Si, which appeared in the Ohio and Wellman material.

The causes of the foregoing differences in microstructure could not be positively identified. However, these differences may arise from: differences in solidification rates, differences in solution heat treating and aging conditions, and differences in the use of sodium additions which modify the morphology of eutectic silicon particles.

Three suggestions were made for non-destructive evaluation methods which might be useful for evaluating the susceptibility to cracking of cylinder barrels in the field. These suggestions were: 1) in situ metallographic examination of cylinder barrels, 2) fracture surface analysis of a small sacrifical specimen, and 3) chemical analysis of a small sacrifical specimen.

VI. ACKNOWLEDGEMENTS:

Mr. C. H. Brady provided valuable skill and assistance with the bulk of the metallographic work. Mr. T. R. Shives provided assistance with the SEM and obtained the photos in Figure 9. Mr. L. C. Smith assisted with manuscript preparation and obtained the photos in Figures 5b and 8. Mr. D. B. Ballard obtained Figures 7, 10a and 10b. Fruitful discussion with Dr. W. J. Boettinger about the interpretations of some of the microstructures is gratefully acknowledged.

BIBLIOGRAPHY

1. Metals Handbook, Eighth Edition. American Society for Metals, Metals Park, Ohio.

   (a) "forging and casting", vol. 5, 1970. Table I on p. 399.

   (b) "metallography, structures and phase diagrams", vol. 8, 1973. Aluminum-Magnesium-Silicon Ternary Phase Diagram on p. 396.

   (c) Aluminum-Iron-Silicon Ternary Phase Diagram on p. 394 of Reference 1b.

   (d) "atlas of microstructures of industrial alloys", Figures 2120 to 2129 on pp. 257, 258.

2a. Specification: Mil H-6088E, "Heat Treatment of Aluminum Alloys", 9 June, 1972.

2b. Specification: Mil A-21180C, "Aluminum Alloy Castings, High Strength", 26 February, 1965.

3. "Optical Microscopy of Casting Alloys", described on p. 68 of Chapter 3 in Aluminum, Vol. 1, (Properties, Physical Metallurgy and Phase Diagrams). Edited by K. R. Van Horn. American Society for Metals, Metals Park, Ohio. 1967.

4. "Eutectic melting and high temperature oxidation", described on p. 353 (also p. 340) of Chapter 9 in Aluminum, Vol. III (Fabrication and Finishing). Edited by K. R. Van Horn. American Society for Metals, Metals Park, Ohio, 1967.

5. Metals Handbook, Eighth Edition (1964), Vol. 2, "heat treating, cleaning and finishing". Figure 2 on p. 272.

6. Metals Handbook, Eighth Edition (1972), Vol. 7, "atlas of microstructures of industrial alloys". Figures 2127 and 2128, p. 258.

7. "Premium-Quality Aluminum Castings", DMIC Report 211, Jan., 1965. Battelle Memorial Institute, Columbus, Ohio 43201

8. M. C. Flemmings: "Solidification of Polyphase Alloys: Castings and Ingots", pp. 181-182 in Chapter 6 of Solidification Processing. McGraw-Hill, New York, 1974.

9. Metals Handbook, Eighth Edition (1972), Vol. 7, "atlas of microstructures of industrial alloys". Figures 2125, 2126 and 2128 on p. 258.

10. G. N. Reinemann and L. E. Marsh: Metals Progress 76 (1), 80-86. (July, 1959).

11. R. A. Zuech: Iron Age 183, 88 (Jan. 29, 1959).

12. T. A. Welsko, D. B. Ballard and M. R. Meyerson: "Tagging of Metal Objects", NBS Report No. 9482 to U.S. Arms Control and Disarmament Agency, April, 1967.

Table I

Room Temperature Tensile Properties of Specimens Taken From Sand Cast and Heat Treated A-356 Cylinder Barrels+

Source of Specimens		Condition*	Specimen Location**	0.2% Offset Yield Strength (psi)	Ultimate Tensile Strength (psi)	Elongation to Fracture (in 1-inch)
Ohio	S/N 8285	a	A	33,300	35,700	1.0%
	8285	a	B	34,400	38,200	1.5
	8285	a	C	32,800	36,600	1.0
	8040	b	A	27,900	34,500	1.4
	8040	b	B	28,300	32,700	1.5
	8040	b	C	27,800	33,500	1.8
	8107	c	A	33,600	38,400	0.7
	8107	c	B	35,500	39,200	0.6
	8107	c	C	31,100	37,200	0.4
Wellman	S/N 4032	d	A	30,300	43,300	5.8%
	4032	d	B	34,500	42,300	5.6
	4032	d	C	32,800	37,500	3.5
Military Specification for Class I, A-356 Castings (Ref. 2b)				28,000 min.	38,000 min.	5.0% elongation in 2-inches

+ These data were provided by the Naval Ordnance Laboratory.

* Key: a - rough machined; no cracks. b - crack detected prior to engine test. c - crack detected after engine test. d - no cracks.

** Key: A - radial. B - axial, at 90° to location A. C - region between two cylinders. Tensile axis parallel to cylinder axis.

Table II

Summary of Eutectics Which May Form In A-356 Alloys*

Type of Eutectic	Solid Phases	Eutectic Temperature (°F)	(°C)
Ternary	Al_{tss}**, Mg_2Al_3, Mg_2Si (rosette)	1038	559
Binary	Al_{tss}, Si_{tss} (particles of eutectic silicon in interdendritic regions)	1071	577
Quasi-Binary	Al_{tss}, Mg_2Si	1103	595

* Reference: Metals Handbook, Eighth Edition (1973), Vol. 8, "metallography, structures and phase diagrams", p. 396.

** The subscript, "tss", signifies terminal solid solution.

Table III

List of Metallographic Specimens From Sand Cast and Heat Treated A-356 Cylinder Barrels

Source of Specimens	Specimen Number	Location on Casting
Specimens Prepared at NOL from Specified Location on Cylinder Barrels from Ohio Foundry	8107*	1[a]
	8107	2[b]
	8107	3[c]
	8040*	1
	8040	3
	8285*	1
	8285	2
Specimens Prepared at NBS from Fractured Tensile Bars	8107B (Ohio)	-
	4032A (Wellman)	-

* Re-polished and re-etched at NBS.

a Adjacent to drilled hole for pin.

b Adjacent to cylinder

c Near outer surface

Figure Legends

1. Solution-treated and aged microstructure of A-356 casting alloy. (a) Regions of primary aluminum solid solution (white), network of eutectic silicon particles in the interdendritic regions (gray), interdendritic shrinkage pores (black) and clusters of Mg_2Si particles (apparent smudges in primary aluminum). (Ohio material: Specimen Number 8107-1.) (b) Close-up of Mg_2Si particles, and eutectic silicon platelets. (Ohio material: Specimen Number 8040-1.)

2. Comparison of typical microstructures in solution-treated and aged A-356 casting alloys. (a) Ohio material: (Specimen Number 8107B, cut from tensile bar.) (b) Wellman material: (Specimen Number 4032A, cut from tensile bar.)

3. Comparison of eutectic silicon particles in solution-treated and aged A-356 casting alloys. (a) Ohio material: (Specimen Number 8040B-1.) (b) Wellman material: (Specimen Number 4032A.)

4. Comparison of Mg_2Si particles in solution-treated and aged A-356 casting alloys. (a) Ohio material: (Specimen Number 8107B, cut from tensile bar.) (b) Wellman material: (Specimen Number 4032A, cut from tensile bar.)

5. Natural crack paths in Ohio material. (a) Near surface and between two rounded black features thought to be embedded particles of sand. (Specimen Number 8040-1.) (b) Edge-on view of crack near drilled hole. (Specimen cut from casting near drilled hole.) See also Figure 6.

6. Close-up of near-surface crack appearing in Figure 5a. (Ohio material: Specimen Number 8040-1.)

7. Typical crack path on as-machined surface. View of the interior of a sectioned hole which was drilled to accommodate a pin. (Ohio material: Specimen cut from casting near drilled hole.) Contrast due to topography, not etching.

8. Examples of how crack path follows eutectic silicon particles in Ohio material. (a) Primary crack and associated secondary cracks. (b) Close-up of secondary crack showing fracture of silicon particles. (Specimen cut from casting near drilled hole.)

9. SEM views of the fracture surface of a natural crack in Ohio material. (a) Large cleavage facet. (b) Interdendritic shrinkage pores, and cleavage facets. (c) Voids due to pull-out of silicon particles, and cleavage facets. (Specimen cut from casting near drilled hole.)

10. Fracture surfaces of tensile bars. (a) Cleavage facets and an interdendritic shrinkage pore in Ohio material, as viewed in SEM. (b) Cleavage facets in Wellman material, as viewed in SEM. (c) Brightly reflecting cleavage facets in Ohio material. (d) Faintly reflecting cleavage facets in Wellman material. (Ohio material: Specimen Number 8107B. Wellman material: Specimen No. 4032A.)

11. Rosettes interpreted as evidence of ternary eutectic phases. (a) and (b) Rosettes embedded in primary aluminum solid solution. The needle-like and blade-like particles are thought to be $Fe_2Si_2Al_9$. (c) Non-rosette shaped regions thought to contain ternary eutectic phases. (Ohio material: Specimen Number 8107B-1.)

12. Triangular regions interpreted as evidence of binary eutectic melting. (Ohio material: Specimen Number 8040B-1.)

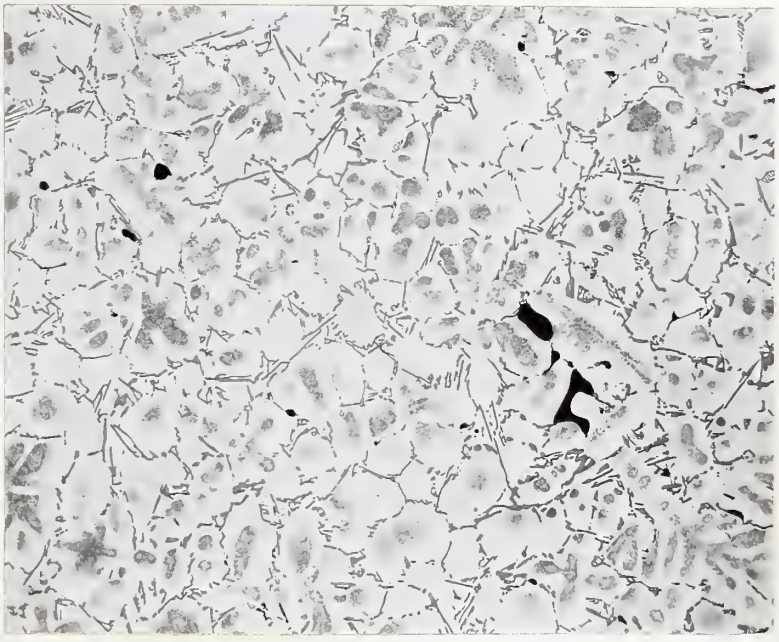

Etchant: 1% HF 50X

(a)

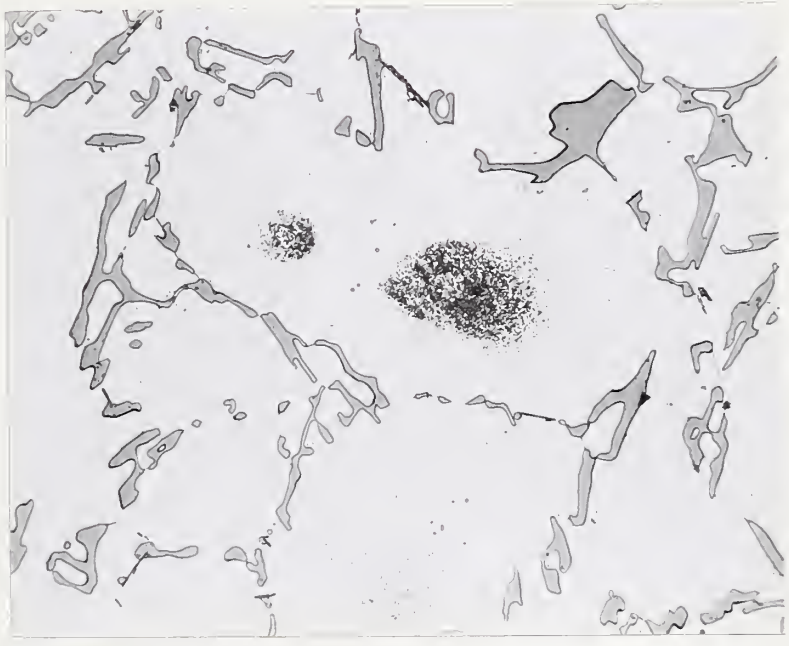

Etchant: 1% HF 250X

(b)

Figure 1. Solution-treated and aged microstructure of A-356 casting alloy. (a) Regions of primary aluminum solid solution (white), network of eutectic silicon particles in the interdendritic regions (gray), interdendritic shrinkage pores (black) and clusters of Mg_2Si particles (apparent smudges in primary aluminum). (Ohio material: Specimen Number 8107-1.) (b) Close-up of Mg_2Si particles, and eutectic silicon platelets. (Ohio material: Specimen Number 8040-1.)

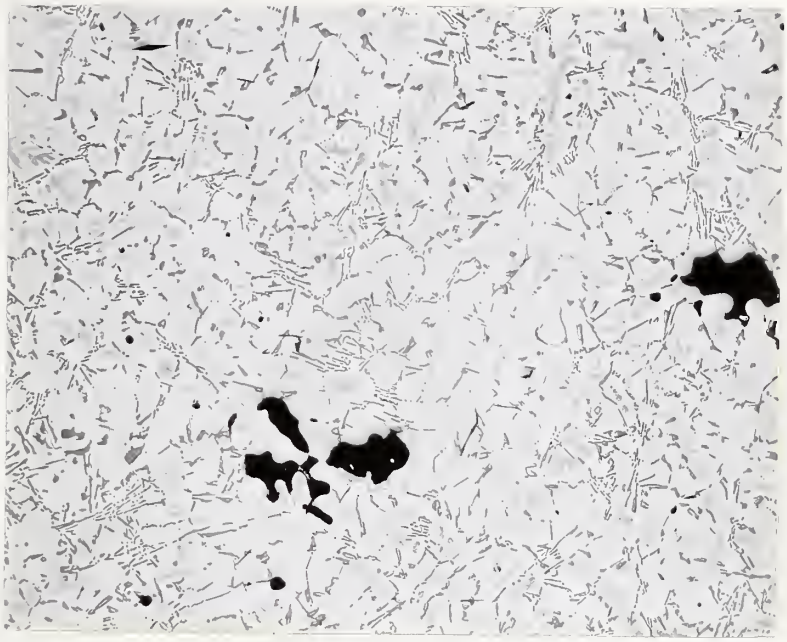

Etchant: 1% HF 50X

(a)

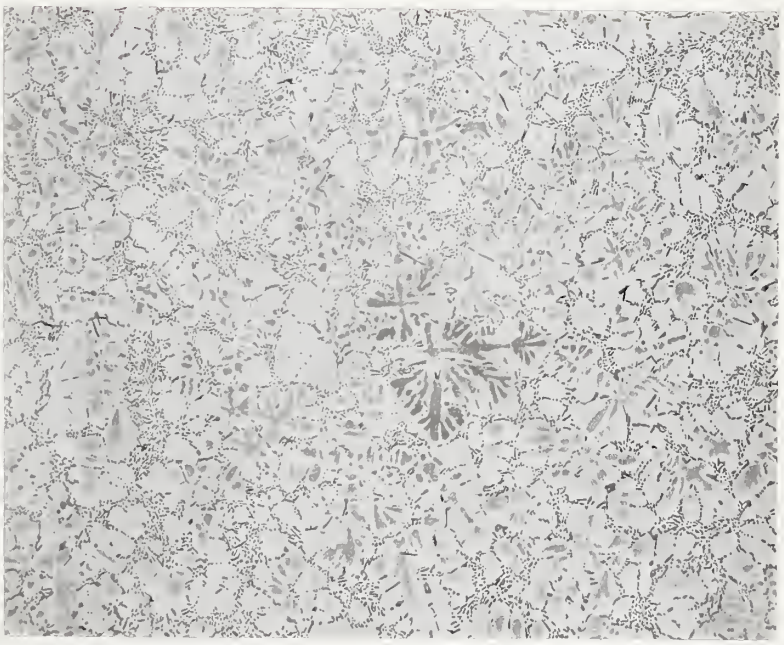

Etchant: 1% HF 50X

(b)

Figure 2. Comparison of typical microstructures in solution-treated and aged A-356 casting alloys. (a) Ohio material: (Specimen Number 8107B, cut from tensile bar.) (b) Wellman material: (Specimen Number 4032A, cut from tensile bar.)

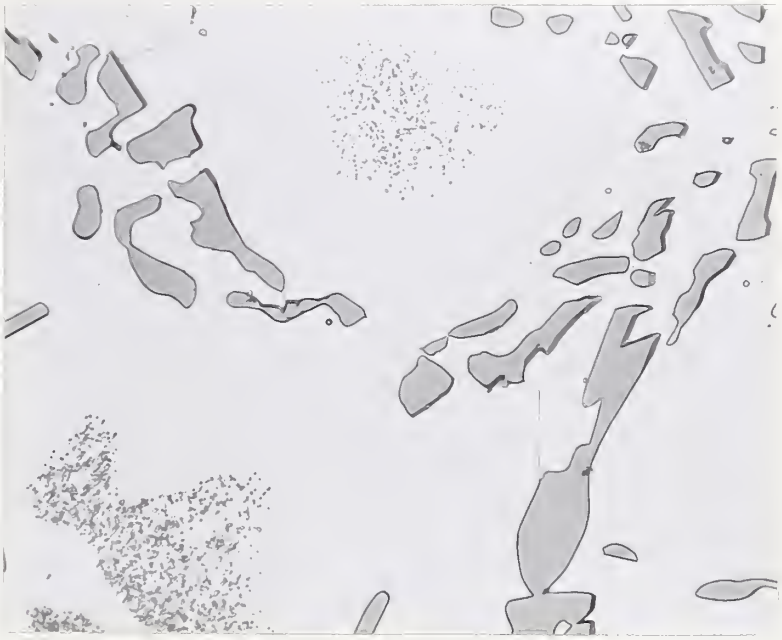

Etchant: 1% HF 500X

(a)

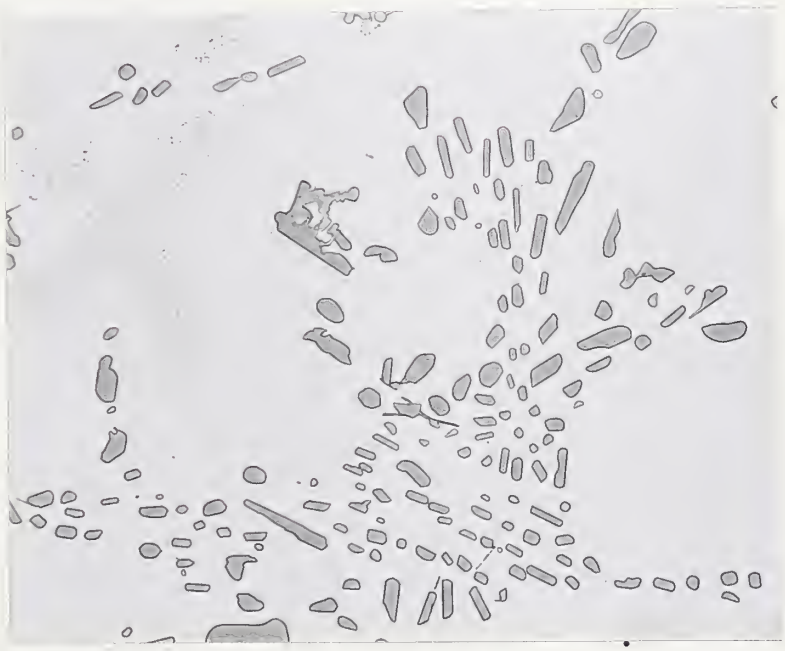

Etchant: 1% HF 500X

(b)

Figure 3. Comparison of eutectic silicon particles in solution-treated and aged A-356 casting alloys. (a) Ohio material: (Specimen Number 8040B-1.) (b) Wellman material: (Specimen Number 4032A.)

Etchant: 1% HF 1500X

(a)

Etchant: 1% HF 1500X

(b)

Figure 4. Comparison of Mg_2Si particles in solution-treated and aged A-356 casting alloys. (a) Ohio material: (Specimen Number 8107B, cut from tensile bar.) (b) Wellman material: (Specimen Number 4032A, cut from tensile bar.)

As Polished 50X

(a)

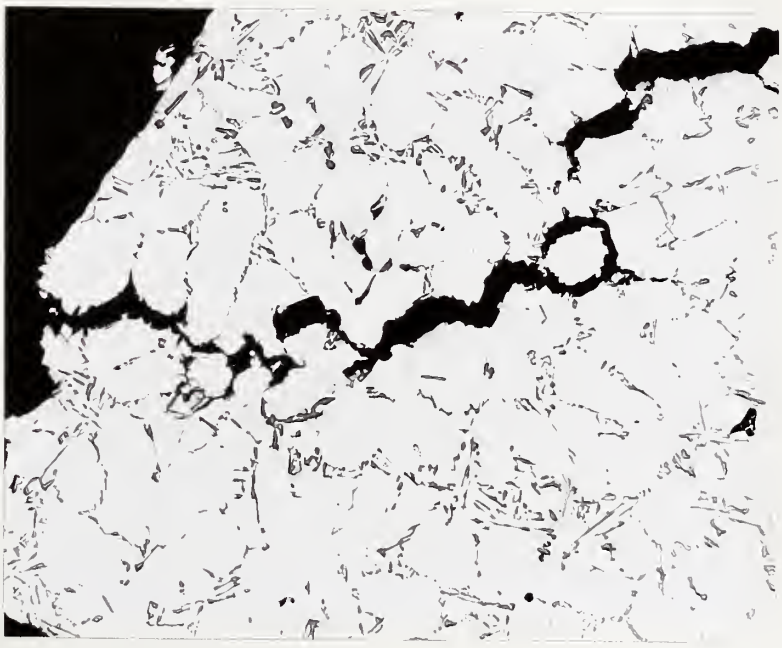

As Polished 50X

(b)

Figure 5. Natural crack paths in Ohio material. (a) Near surface and between two rounded black features thought to be embedded particles of sand. (Specimen Number 8040-1.) See also F
(b) Edge-on view of crack near drilled hole. (Specimen cut from casting near drilled hole.)

As Polished 250X

Figure 6. Close-up of near-surface crack appearing in Figure 5a. (Ohio material: Specimen Number 8040-1.)

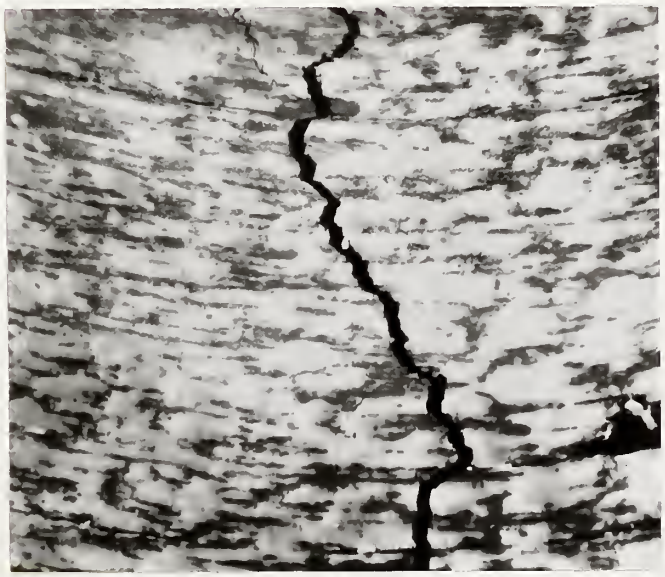

As Machined 75X

Figure 7. Typical crack path on as-machined surface. View of the interior of a sectioned hole which was drilled to accommodate a pin. (Ohio material: Specimen cut from casting near drilled hole.)

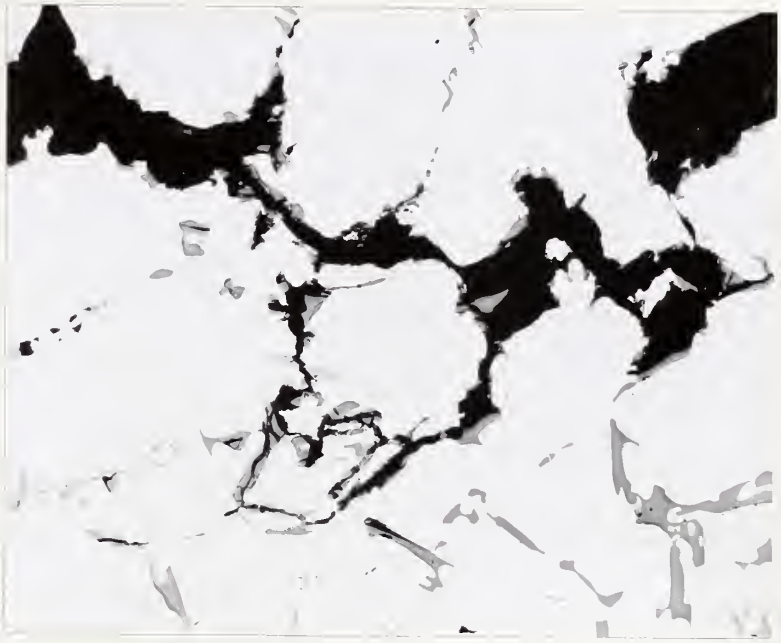

As Polished 200X

(a)

As Polished 500X

(b)

Figure 8. Examples of how crack path follows eutectic silicon particles in Ohio material. (a) Primary crack and associated secondary cracks. (b) Close-up of secondary crack showing fracture of silicon particles. (Specimen cut from casting near drilled hole.)

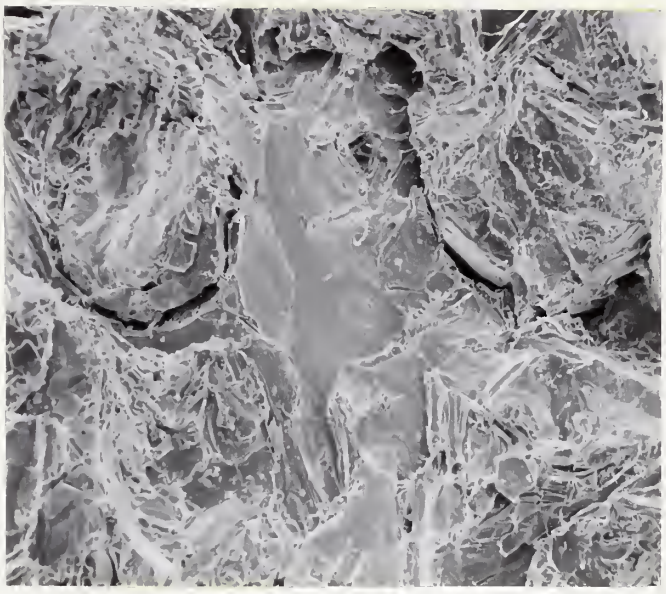

As Fractured 180X

(a)

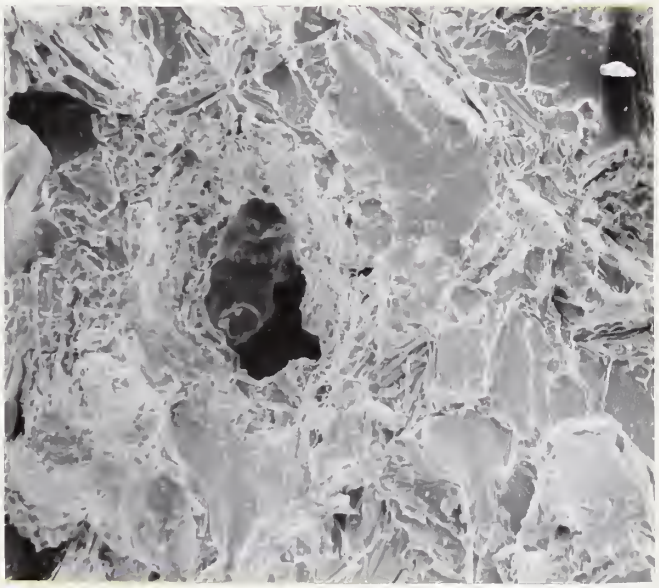

As Fractured X170X

(b)

Figure 9. SEM views of the fracture surface of a natural crack in Ohio material. (a) Large cleavage facet. (b) Interdendritic shrinkage pores, and cleavage facets. (Specimen cut from casting near drilled hole.)

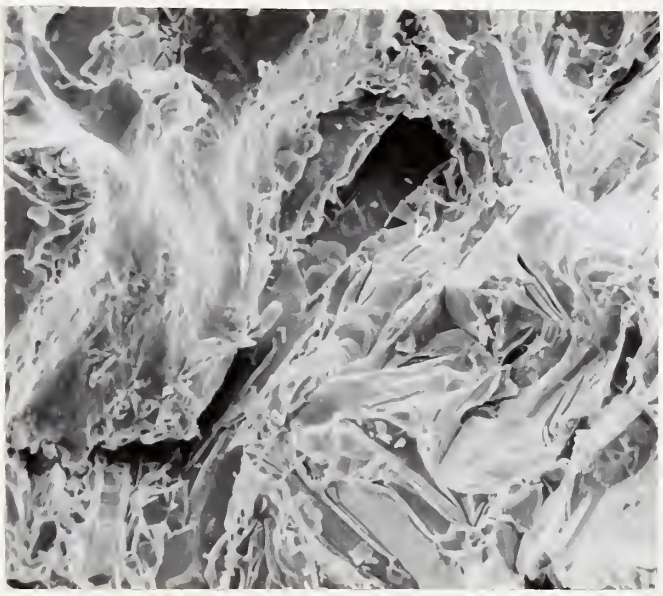

As Fractured 430X

(c)

Figure 9c. Voids due to pull-out of silicon particles, and cleavage facets. (Ohio material: Specimen cut from casting near drilled hole.)

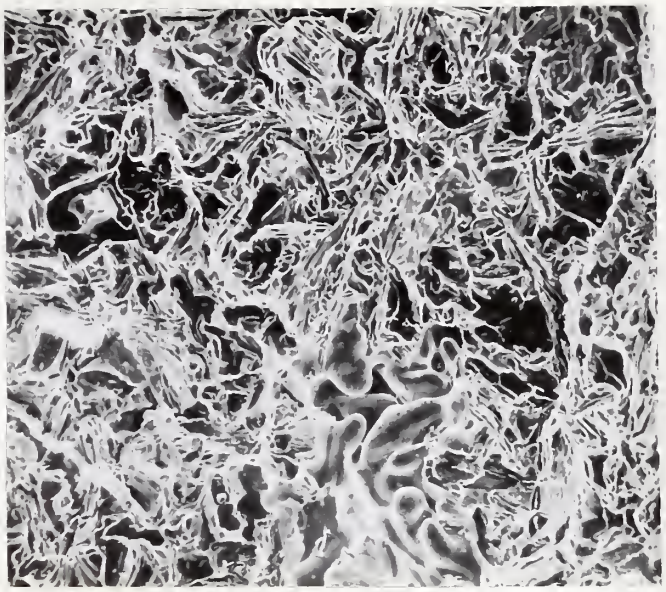

As-Fractured 112X

(a)

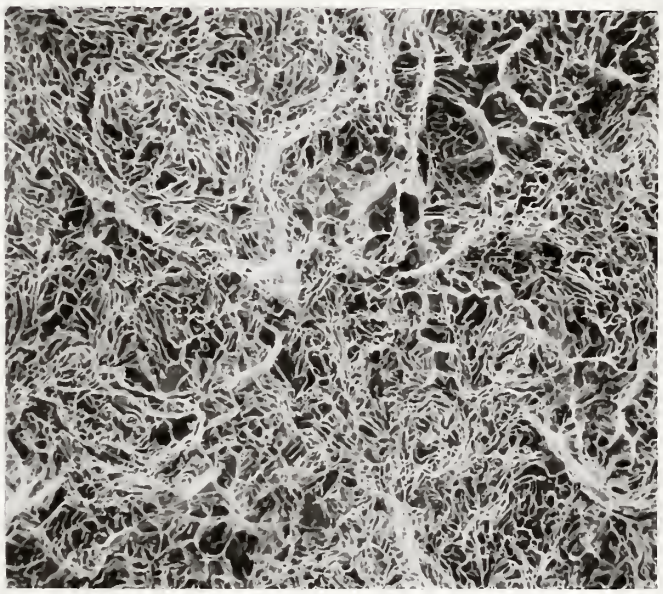

As-Fractured 112X

(b)

Figure 10. Fracture surfaces of tensile bars. (a) Cleavage facets and an interdendritic shrinkage pore in Ohio material, as viewed in SEM. (Specimen Number 8107B.) (b) Cleavage facets in Wellman material, as viewed in SEM. (Specimen Number 4032A.)

As-Fractured 6X

(c)

As-Fractured 6X

(d)

Figure 10. Fracture surfaces of tensile bars. (c) Brightly reflecting cleavage facets in Ohio material. (Specimen Number 8107B.) (d) Faintly reflecting cleavage facets in Wellman material. (Specimen Number 4032A.)

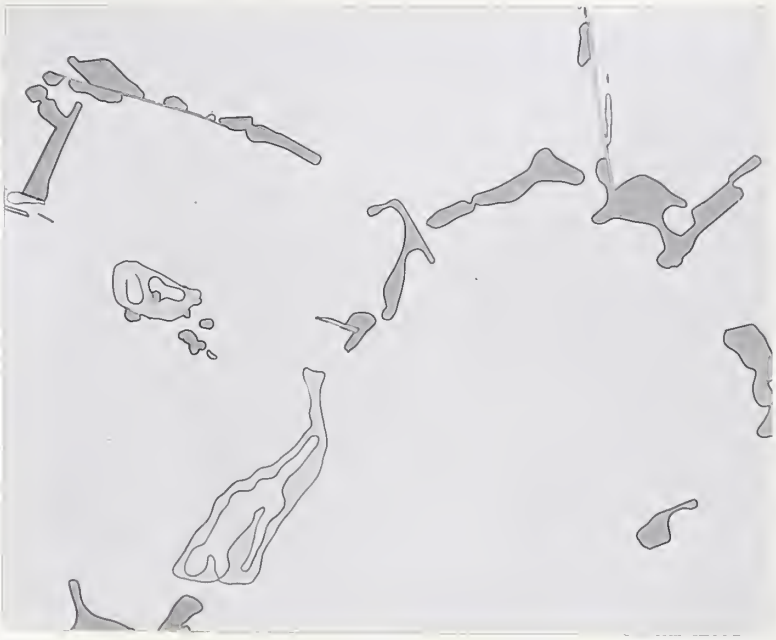

Etchant: 1% HF 500X

(a)

Etchant: 1% HF 500X

(b)

Figures 11a and 11b. Rosettes interpreted as evidence of ternary eutectic phases. Rosettes embedded in primary aluminum solid solution. The needle-like and blade-like particles are thought to be $Fe_2Si_2Al_9$. (Ohio material: Specimen Number 8107B-1.)

Etchant: 1% HF 500X

(c)

Figure 11c. Non-rosette shaped regions thought to contain ternary eutectic phases. (Ohio material: Specimen Number 8107B-1.)

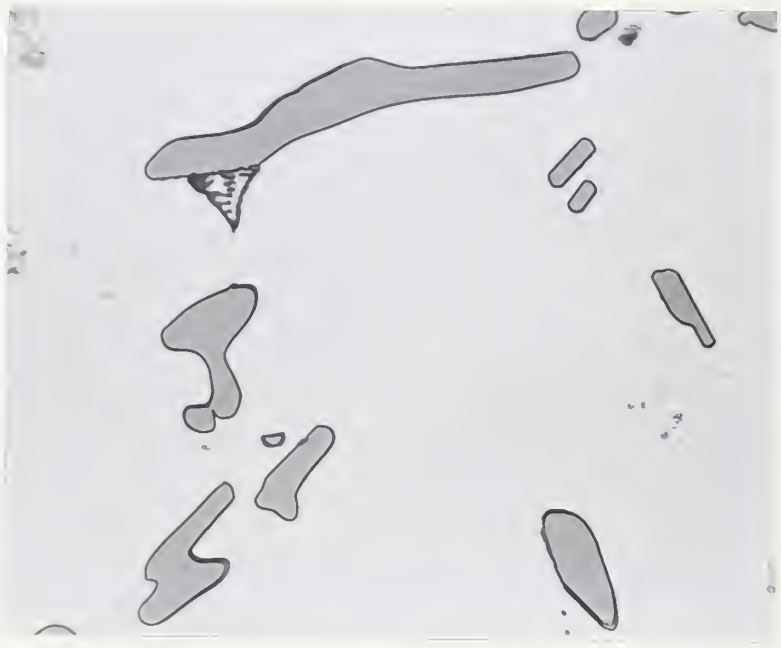

Etchant: 1% HF 1000X

Figure 12. Triangular regions interpreted as evidence of binary eutectic melting. (Ohio material: Specimen Number 8040B-1.)

U.S. DEPT. OF COMM. BIBLIOGRAPHIC DATA SHEET	1. PUBLICATION OR REPORT NO. NBSIR 74-579	2. Gov't Accession No.	3. Recipient's Accession No.

4. TITLE AND SUBTITLE

METALLOGRAPHIC EXAMINATION OF CYLINDER BARRELS MADE FROM ALUMINUM ALLOY (A-356) SAND CASTINGS

5. Publication Date: September 1974

6. Performing Organization Code

7. AUTHOR(S): B. W. Christ

8. Performing Organ. Report No. NBSIR 74-579

9. PERFORMING ORGANIZATION NAME AND ADDRESS

NATIONAL BUREAU OF STANDARDS
DEPARTMENT OF COMMERCE
WASHINGTON, D.C. 20234

10. Project/Task/Work Unit No. 3120586

11. Contract/Grant No.

12. Sponsoring Organization Name and Complete Address (Street, City, State, ZIP)

Naval Ordnance Laboratory
White Oak, Silver Spring, Md. 20910

13. Type of Report & Period Covered: Failure Analysis Report

14. Sponsoring Agency Code

15. SUPPLEMENTARY NOTES

16. ABSTRACT (A 200-word or less factual summary of most significant information. If document includes a significant bibliography or literature survey, mention it here.)

A metallographic examination was carried out on cylinder barrels made from aluminum alloy (A-356) sand castings. Some castings exhibited a tendency to crack during machining and/or testing. The examination revealed that cracks propagated through large eutectic silicon platelets in the interdendritic regions. Possible origins of the large eutectic silicon platelets were discussed. Some suggestions were made about non-destructive evaluation methods which would help to identify castings with a potential for cracking.

17. KEY WORDS (six to twelve entries; alphabetical order; capitalize only the first letter of the first key word unless a proper name; separated by semicolons)

A-356 aluminum; eutectic silicon platelets; interdendritic shrinkage; non-destructive evaluation, sand casting; yield and ultimate tensile strengths.

18. AVAILABILITY

[ ] Unlimited

[X] For Official Distribution. Do Not Release to NTIS

[ ] Order From Sup. of Doc., U.S. Government Printing Office Washington, D.C. 20402, SD Cat. No. C13

[ ] Order From National Technical Information Service (NTIS) Springfield, Virginia 22151

19. SECURITY CLASS (THIS REPORT)	21. NO. OF PAGES
UNCLASSIFIED	32
20. SECURITY CLASS (THIS PAGE)	22. Price
UNCLASSIFIED	